Available online at www.sciencedirect.com
ScienceDirect
International Journal of Thermal Sciences 47 (2008) 25–34
International Journal of Thermal Sciences
www.elsevier.com/locate/ijts

Sinusoidal perturbation solution for solidification of pure materials on a planar mold of finite thickness

Faruk Yigit

Department of Mechanical Engineering, King Saud University, P.O. Box 800, Riyadh 11421, Saudi Arabia

Received 18 March 2006; received in revised form 14 January 2007; accepted 15 January 2007

Available online 22 February 2007

Abstract

A linear perturbation method is used to solve two-dimensional heat conduction problem in which a liquid becomes solidified by heat transfer to a plane mold of finite thickness. Heat flux drawn from the lower surface of the mold is approximately uniform, but contains a small sinusoidal perturbation in one space dimension. Numerical results are obtained for the consequent sinusoidal perturbation in the solid/melt boundary as a function of time. Analytical results are obtained for the limiting case in which diffusivities of the solidified shell and the mold materials are infinitely large. These results are then compared with the numerical predictions to establish the validity of the model and the numerical approach. The results document the effects of both solidified shell and the mold material diffusivities on the growth of a perturbation in a nominally plane solidification front. It is demonstrated that the magnitude of this perturbation increases with the diffusivity of the mold, and this effect of mold diffusivity is overweighed by the diffusivity of the casting material. The influence of other process parameters such as the mold thickness, thermal contact resistance at the mold–shell interface, and thermal conductivity ratio on the growth of solidified shell thickness is also investigated in detail.

Keywords: Solidification; Growth; Instability; Phase-change; Perturbation

1. Introduction

Problems of heat transfer accompanied by a phase change (Stefan problems) are encountered in many areas of applied science such as the process of casting, recrystallization of metals, welding, evaporation of droplets, oxygen diffusion problems, and the formation of ice [1]. The complexity of these problems is due to the nonlinear boundary conditions at the solid/melt moving interface. Solution of the Stefan problems requires simultaneous determination of the shape and the motion of this moving front along with the temperature fields in the solidified shell and the mold. Exact solutions for the Stefan problems are known only in a few special cases [2,3]. Neumann's solution to the one-dimensional problem of solidification in a semi-infinite region is one of the most well-known exact solutions. Approximate analytical solutions have been obtained by a variety of techniques, such as the use of the heat balance [4–6] and coupled integral equation methods [7,8]. Many problems have also been investigated with numerical methods, notably the finite difference [9,10] and finite element methods [11,12]. Perturbation methods have also been successfully applied to Stefan problems with simple boundary conditions in different geometries. The perturbation solutions for the planar solidification of a saturated liquid with convection at the wall has been found by Pedroso and Domoto [13]. On the other hand, Pedroso and Domoto [14], and Stephan and Holzknecht [15] have found the perturbation solutions for outward spherical and cylindrical solidifications. Caldwell and Kwan [16] have developed the perturbation methods for the phase change problems with time-dependent boundary conditions. Yang et al. [17] have been solved a one-dimensional solidification problem in a finite domain using perturbation methods with the Stefan number as the small parameter. Charach et al. [18] developed a perturbation method for the analysis of weakly nonlinear Stefan problems with time-dependent temperature boundary conditions. A regular perturbation analysis of the one-phase problem for convective and radiative cooling has been carried out by Yang and

E-mail address: fyigit@ksu.edu.sa.

1290-0729/$ – see front matter
doi:10.1016/j.ijthermalsci.2007.01.016

Nomenclature

h	mold thickness	m
K	conductivity	W/m °C
L	latent heat of fusion	Ws/kg
m	$2\pi/\lambda$	1/m
R_0	thermal contact resistance	°C m^2/W
t	time	s
T	temperature	°C
T_m	melting temperature	°C
f_0	initial mold temperature	°C
s	solidified shell thickness	m
Q	heat flux	W/m^2
x, y	Cartesian coordinates	
Y	dimensionless Cartesian coordinate	
S	dimensionless solidification front	
H	dimensionless mold thickness	
$\bar{T}$	dimensionless temperature	
$\bar{Q}$	dimensionless heat flux	
R	dimensionless thermal contact resistance	
N	number of node elements	

Subscripts

0, 1	zeroth and first order, respectively

Superscripts

c, d	shell and mold materials, respectively

Greek symbols

α	diffusivity	m^2/s
ε_1, ε_2	dimensionless specific heats of shell and mold materials, respectively	
λ	wavelength	m
ρ	density	kg/m^3
β	dimensionless time	
ζ	dimensionless conductivity ratio between the shell and mold materials	
δ	space step size	
τ	time increment	
Δ	dimensionless parameter defined by Eq. (50)	

Huang [19]. Significant progress for the two-phase problem in a finite domain reported by Weinbaum and Jiji [20]. Kharche and Howarth [21] considered the inward solidification of liquid cylinders whose boundary values vary slightly with position axially and periodically along the cylinder. They used a linear perturbation method in their solutions. They also investigated a related problem [22], where the boundary profile of the cylinder geometry itself instead of boundary temperature (or heat flux) assumed to vary slightly and periodically with the axial coordinate. Very recently, Yigit [23] applied a linear perturbation technique to solve a two-dimensional heat conduction problem in which a liquid, becomes solidified by heat transfer to a sinusoidal mold with a finite thickness. Unlike the present model, the heat flux drawn from the bottom of the mold was assumed to be uniform and constant. The effect of mold surface wavelength on the growth of the shell for different shell–mold systems was investigated.

As far as melting and solidification problems with grid movements are concerned, comprehensive reviews are available in the literature [24–26]. Caldwell and Kwan [24] described and compared several effective methods for the numerical solution of one-dimensional Stefan problems. Javierre et al. [25] provided a comparison of several numerical methods such as moving grid, the level set, and the phase field to address the suitability of the methodologies. Jana et al. [26] developed a numerical methodology based on the curvilinear, boundary-fitted, finite-volume method for solidification and melting problems for pure substances.

In the casting processes, solidification is affected by heat transfer from melt through the mold to the surroundings. The process therefore generally starts at the mold surface and a shell of solidified material grows from this surface towards the center of the casting. The growth of this shell is often found to be nonuniform [27], even in nominally one-dimensional plane cast surface. This nonuniform shell growth could be a response to a pre-existing nonuniformity in the heat flux drawn from the mold surface. Small spatial perturbations in heat extraction, resulting from oxide films carried on the molten material surface, isolated impurities, or mold surface topography, for example, can lead to shell growth instability during solidification of metals [27]. This is a condition where shell distortion promotes gap nucleation beneath the thinnest regions of the shell while simultaneously enhancing heat extraction beneath the thickest regions of the shell due to improved contact. If solidification process is interrupted, periodic thickness nonuniformities at the freezing front are often observed that can have wavelengths of order of several centimeters [28]. If solidification is allowed to proceed, however, the nonuniformities tend to die out as the freezing front morphology becomes less dependent upon the mold–shell interface due to ever-thickening shell. When the completed casting is sectioned, periodic undulation of the casting microstructure is often observed [28]. Such microstructures are often detrimental to subsequent forming processes and have been linked to severe ingot cracking. It should be however noted that the heat flux itself is also influenced by the contact conditions between the shell and the mold. Thus, it is possible that a small spatial perturbation in the heat flux could be unstable due to thermomechanical coupling. Instabilities of this kind have already been reported in many experimental and theoretical studies [29,30]. Theoretical models of the proposed growth instability mechanism during solidification of pure metals have been presented by Richmond et al. [31], Li and Barber [32], and later extended by Yigit and Hector [33,34], Hector et al. [35], and Yigit [36].

Each of the previous theoretical growth instability models neglect either the thermal properties of the mold completely or the thermal capacitance of the solidifying shell material. None

of the studies except [23] cited above examined the combined effects of nonzero thermal capacities of the shell and mold materials. This paper seeks to enhance our knowledge about the effects of these two important thermal properties on the growth instability observed in many casting processes using a specifically designed heat conduction model. In particular, it addresses the interaction of these parameters against each other, and extends earlier investigations to determine process parameters which are most favored for growth instability. Thus, it can be considered as a first step to obtain a complete thermo-mechanical model for the aforementioned instability mechanism. The present heat conduction model can be combined to a thermo-elastic deformation model to determine the development of the residual stresses and the contact pressure to examine the stability of thermoelastic contact problem since the perturbation method described here provides stability criterion which models the physics of the growing solid and its deformation. Earlier models of solidification thermo-mechanics suggest that growth instability can be minimized or completely avoided by a careful choice of process parameters such as the shell and mold materials Stefan number, conductivity ratios, the mold thickness, and wavelength of the cooling profile. The suggested model in the present work enable us to investigate how the variation of heat flux might affect the solidification rate and the thickness nonuniformity. For this purpose, a numerical solution is developed for a specifically designed heat conduction model where one-dimensional solidification is perturbed by the superposition of a small spatial sinusoidal variation in heat flux. In particular, we obtain solutions for the temperature fields in the shell and the mold, and the advance of the solid/melt boundary. Once the temperature fields are known, the thermoelastic stress fields can then be determined following the same perturbation approach outlined in [37]. We also briefly discuss the effect of thermal diffusivities of the solidified shell and the mold materials, the mold thickness, the thermal contact resistance at the solid-shell interface, and the thermal conductivity ratio on the growth of solidified shell thickness.

2. Mathematical formulation

We consider the two-dimensional problem of a liquid initially at its melting temperature T_m, in contact with a mold of thickness h. The present model is restricted to the solidification of pure materials. Therefore, there is no mushy zone between liquid and solid phases, and the solidification occurs at a distinct temperature rather than over a range of temperatures. The liquid phase being at the uniform melting temperature T_m throughout, there is no heat transfer through it; the heat released during solidification process is transferred into the mold, and raises its temperature. Solidification starts by the formation of a shell adjacent to the shell–mold interface, since this is the coolest part of the liquid mass. Subsequent cooling requires that heat be conducted through this layer and across the shell–mold interface. Hence, temperature distributions are unknowns only in the solidified shell and the mold. After a time t, the liquid solidified near the mold forms a solid shell thickness $s(x,t)$. Thus, $s(x,t)$ defines the moving interface between the solid and liquid phases as shown in Fig. 1. We assume that densities ρ^c, ρ^d, thermal diffusivities α^c, α^d, and conductivities K^c, K^d of the solid phase and the mold are constant and independent of temperature and time. The temperature of the solidified shell and the mold $T^c(x,y,t)$, $T^d(x,y,t)$ must satisfy the heat conduction equations:

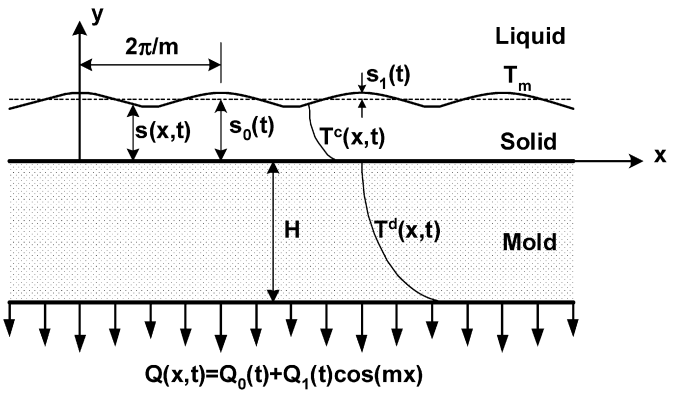

Fig. 1. Geometry of nonuniform unidirectional solidification.

$$\nabla^2 T^c(x,y,t) = \frac{1}{\alpha^c}\frac{\partial T^c}{\partial t}(x,y,t)$$

$$\nabla^2 T^d(x,y,t) = \frac{1}{\alpha^d}\frac{\partial T^d}{\partial t}(x,y,t), \quad t>0 \tag{1}$$

which are subject to the following boundary conditions:

$$T^c(x,s,t) = T_m \tag{2}$$

$$K^c\frac{\partial T^c}{\partial y}(x,s,t) = L^c\rho^c\frac{\partial s}{\partial t}(x,t) \tag{3}$$

$$K^c\frac{\partial T^c}{\partial y}(x,0,t) = K^d\frac{\partial T^d}{\partial y}(x,0,t) \tag{4}$$

$$K^c\frac{\partial T^c}{\partial y}(x,0,t) = \frac{1}{R_0}\left[T^c(x,0,t) - T^d(x,0,t)\right] \tag{5}$$

$$K^d\frac{\partial T^d}{\partial y}(x,-h,t) = Q(x) \tag{6}$$

where L^c is the latent heat of fusion of the solidified material and R_0 is the thermal contact resistance at the mold/solid interface.

Eq. (2) states that the freezing front is isothermal at the fusion temperature, while (3) defines an energy balance between the heat conducted away from the moving interface into the solidified shell and the latent heat released during solidification. Eq. (4) states that heat flux from the casting to the mold must be continuous. Heat flux from the casting to the mold is modeled by a thermal contact resistance R_0, as described by the boundary condition (5), due to the presence of air gaps and/or inclusions of materials of poor conductivity at the mold–shell interface. Finally, Eq. (6) prescribes heat flux drawn from the lower surface of the mold.

3. The perturbation analysis

If the mold is at uniform temperature, there is clearly a one-dimensional solution to the problem described above, in

which the solidification front at any given time is defined by the straight line $y = s_0(t)$ and all physical quantities are functions of y, t, but are independent of x. If an x-dependent perturbation is to grow on this unperturbed or 'zeroth order' process, its development will be influenced by the instantaneous zeroth order quantities. As long as the perturbation is small compared with the zeroth order values, the perturbation will be linear, and permits us to use Fourier transformation in x. This has the effect of reducing the dimensionality of the problem. Since the zeroth and first order problems involve fields varying in only one spatial dimension and time, they are considerably easier to implement and more efficient computationally than a full two-dimensional numerical solution of the solidification problem. When the thermal stresses are combined into the heat conduction problem introduced above, essentially, we have to solve a nonlinear problem in y, t to determine the zeroth order solution, after which perturbation problem will define a linear problem in y, t, defined by differential equations with variable coefficients, these being derived by perturbation of the zeroth order equations. Since the nonlinearity of the problem is confined to the zeroth order process, which therefore generally requires a numerical solution, no extra difficulty will be introduced by using a fully nonlinear constitutive law for the material deformation.

The rate of solidification of metals and the resulting properties of the cast product are largely controlled by the physics of the mold–shell interface. In particular, the interfacial heat flux is strongly moderated by contraction of the casting at the mold–shell interface which leads to local air gaps. Consequently, the local heat flux across the gaps becomes distorted since significant heat flow occurs through the solid–solid contacts in comparison to that across the gaps. Additionally, the mold surface might be imperfectly wetted because of surface tension in the molten metal, and therefore solid skin nucleation begins at asperity peaks with micro-air gaps between peaks. This action prevents heat from being extracted uniformly. Experimental observations (see, for example, Fig. 1 of Ref. [28]) indicate that the development of solidification front exhibits sinusoidal perturbations. It is anticipated that this nonuniform shell growth could be a response to a pre-existing nonuniformity in the heat flux drawn from the mold surface. A suitable idealized assumption for this purpose is that both the zeroth and first order heat fluxes at the bottom of the mold surface are prescribed to be constants, Q_0, Q_1 respectively, instead of being determined by the interaction between contact pressure and thermal contact resistance. In fact, this assumption is not very unrealistic particularly for the early times of the process in view of the fact that a strong coupling between the thermal and mechanical fields will be developed at later stages of the solidification (see, for example, [33,34,37]).

We therefore consider the case in which the prescribed heat flux from the lower surface of the mold is of the form

$$Q(x) = Q_0 + Q_1 \cos(mx), \quad y = -h \tag{7}$$

where Q_0 and Q_1 are time-independent constants representing the uniform heat flux and the heat flux perturbation, respectively. The constant m is the wave number that defines the wavelength λ of the perturbation through

$$\lambda = 2\pi/m \tag{8}$$

The perturbation is assumed to be sufficiently small for the corresponding two-dimensional problem that will be solved by a linear perturbation of the zeroth-order solution. Since the perturbation is small, we have $Q_1 \ll Q_0$ and similar inequalities for all the field quantities. As a result of the perturbation we anticipate a corresponding small sinusoidal perturbation in the temperature field and in the solidification front that can be defined by

$$T^i(x, y, t) = T_0^i(y, t) + T_1^i(y, t)\cos(mx)$$
$$T_1^i(y, t) \ll T_0^i(y, t) \quad (i = c, d) \tag{9}$$
$$s(x, t) = s_0(t) + s_1(t)\cos(mx), \quad s_1(t) \ll s_0(t) \tag{10}$$

Notice that temperatures depend on y and t only. Suffix 0 refers to the x-independent zeroth order process, and the problem has a simple one-dimensional solution which is called the "zeroth-order" solution. However, suffix 1 refers to the amplitude of the sinusoidal perturbation or first order process. It is assumed that the amplitude of this perturbation is small in comparison with its wavelength (i.e., $ms_1(t) \ll 1$), in which case the slope of the moving front, $\partial s/\partial x$, is very much less than unity. It then follows that the heat flux in the x-direction is negligible to the first order.

Substituting Eq. (9) into Eq. (1) and separating periodic and uniform terms in x, we obtain

$$\frac{\partial^2 T_0^c}{\partial y^2}(y, t) = \frac{1}{\alpha^c}\frac{\partial T_0^c}{\partial t}(y, t)$$
$$\frac{\partial^2 T_0^d}{\partial y^2}(y, t) = \frac{1}{\alpha^d}\frac{\partial T_0^d}{\partial t}(y, t) \tag{11}$$
$$\frac{\partial^2 T_1^c}{\partial y^2}(y, t) - m^2 T_1^c(y, t) = \frac{1}{\alpha^c}\frac{\partial T_1^c}{\partial t}(y, t)$$
$$\frac{\partial^2 T_1^d}{\partial y^2}(y, t) - m^2 T_1^d(y, t) = \frac{1}{\alpha^d}\frac{\partial T_1^d}{\partial t}(y, t) \tag{12}$$

Since the perturbation is small, we can expand the temperature field in the vicinity of the mean solid/melt interface position, $y = s_0(t)$, in the form of a Taylor series, in which case boundary condition (2) can be written as

$$T_0^c(s_0, t) + \frac{\partial T_0^c(s_0, t)}{\partial y} s_1(t)\cos(mx) + \frac{\partial^2 T_0^c(s_0, t)}{\partial y^2}\frac{s_1^2\cos^2(mx)}{2!} + \left[T_1^c(s_0, t) + \frac{\partial T_1^c(s_0, t)}{\partial y} s_1(t)\cos(mx) + \cdots\right] \times \cos(mx) = T_m \tag{13}$$

Separating periodic and uniform terms and dropping second and higher order and product terms in the small quantities, T_1 and s_1 (i.e., the third and the fifth terms from the left in Eq. (13) can be neglected), we obtain the two first order equations

$$T_0^c(s_0, t) = T_m \tag{14}$$

$$s_1(t)\frac{\partial T_0^c}{\partial y}(s_0, t) + T_1^c(s_0, t) = 0 \tag{15}$$

A similar procedure applied to the boundary condition (3) also yields the two equations

$$L^c\rho^c\frac{ds_0(t)}{dt}=K^c\frac{\partial T_0^c}{\partial y}(s_0,t) \tag{16}$$

$$L^c\rho^c\frac{ds_1(t)}{dt}=K^c\left[\frac{\partial T_1^c(s_0,t)}{\partial y}+s_1(t)\frac{\partial^2 T_0^c(s_0,t)}{\partial y^2}\right] \tag{17}$$

The solid/mold boundary conditions (4) and (5) give

$$K^c\frac{\partial T_0^c}{\partial y}(0,t)=K^d\frac{\partial T_0^d}{\partial y}(0,t) \tag{18}$$

$$K^c\frac{\partial T_1^c}{\partial y}(0,t)=K^d\frac{\partial T_1^d}{\partial y}(0,t) \tag{19}$$

$$R_0K^c\frac{\partial T_0^c}{\partial y}(0,t)=T_0^c(0,t)-T_0^d(0,t) \tag{20}$$

$$R_0K^c\frac{\partial T_1^c}{\partial y}(0,t)=T_1^c(0,t)-T_1^d(0,t) \tag{21}$$

Finally, the boundary condition (6) at the bottom of the mold gives the two equations

$$K^d\frac{\partial T_0^d}{\partial y}(-h,t)=Q_0 \tag{22}$$

$$K^d\frac{\partial T_1^d}{\partial y}(-h,t)=Q_1 \tag{23}$$

Notice that the zeroth order boundary conditions are identical to that for the unperturbed problem, whereas that for the first order includes terms derived from the zeroth order solution. This is typical of the procedure and permits the two problems to be solved sequentially.

4. Dimensionless formulation

Before proceeding to the solution, it is convenient to introduce the following dimensionless variables

$$\begin{aligned}
&Y=my, \qquad S(\beta)=ms(t), \qquad H=mh\\
&\beta=m^2\frac{K^c(T_m-f_0)}{\rho^cL^c}t, \qquad \bar{T}(Y,\beta)=\frac{T(y,t)-f_0}{T_m-f_0}\\
&\bar{Q}=\frac{Q}{mK^c(T_m-f_0)}, \qquad R=mK^cR_0, \qquad \zeta=\frac{K^c}{K^d}\\
&\varepsilon_1=\frac{K^c(T_m-f_0)}{\alpha^c\rho^cL^c}, \qquad \varepsilon_2=\frac{K^c(T_m-f_0)}{\alpha^d\rho^cL^c}
\end{aligned} \tag{24}$$

The governing equations (11) and (12) for $\bar{T}_0^c(Y,\beta)$, $\bar{T}_0^d(Y,\beta)$ and $\bar{T}_1^c(Y,\beta)$, $\bar{T}_1^d(Y,\beta)$ then become

$$\begin{aligned}
&\frac{\partial^2\bar{T}_0^c(Y,\beta)}{\partial Y^2}=\varepsilon_1\frac{\partial\bar{T}_0^c(Y,\beta)}{\partial\beta}\\
&\frac{\partial^2\bar{T}_0^d(Y,\beta)}{\partial Y^2}=\varepsilon_2\frac{\partial\bar{T}_0^d(Y,\beta)}{\partial\beta}
\end{aligned} \tag{25}$$

$$\begin{aligned}
&\frac{\partial^2\bar{T}_1^c(Y,\beta)}{\partial Y^2}-\bar{T}_1^c(Y,\beta)=\varepsilon_1\frac{\partial\bar{T}_1^c(Y,\beta)}{\partial\beta}\\
&\frac{\partial^2\bar{T}_1^d(Y,\beta)}{\partial Y^2}-\bar{T}_1^d(Y,\beta)=\varepsilon_2\frac{\partial\bar{T}_1^d(Y,\beta)}{\partial\beta}
\end{aligned} \tag{26}$$

The dimensionless boundary conditions corresponding to the zeroth order temperature fields $\bar{T}_0^c(Y,\beta)$ and $\bar{T}_0^d(Y,\beta)$ can be obtained using Eqs. (14), (16), (18), (20), (22) as follows:

$$\bar{T}_0^c(S_0,\beta)=1 \tag{27}$$

$$\frac{dS_0(\beta)}{d\beta}=\frac{\partial\bar{T}_0^c(S_0,\beta)}{\partial Y} \tag{28}$$

$$R\frac{\partial\bar{T}_0^c(0,\beta)}{\partial Y}=\bar{T}_0^c(0,\beta)-\bar{T}_0^d(0,\beta) \tag{29}$$

$$R\frac{\partial\bar{T}_0^d(0,\beta)}{\partial Y}=\zeta\left\{\bar{T}_0^c(0,\beta)-\bar{T}_0^d(0,\beta)\right\} \tag{30}$$

$$\frac{\partial\bar{T}_0^d(-H_0,\beta)}{\partial Y}=\zeta\,\bar{Q}_0 \tag{31}$$

The dimensionless boundary conditions corresponding to the first order temperature fields $\bar{T}_1^c(Y,\beta)$ and $\bar{T}_1^d(Y,\beta)$ can be determined using Eqs. (15), (17), (19), (21), (23) as follows:

$$S_1(\beta)\frac{\partial\bar{T}_0^c(S_0,\beta)}{\partial Y}+\bar{T}_1^c(S_0,\beta)=0 \tag{32}$$

$$\frac{dS_1(\beta)}{d\beta}=\frac{\partial\bar{T}_1^c(S_0,\beta)}{\partial Y}+S_1(\beta)\frac{\partial^2\bar{T}_0^c(S_0,\beta)}{\partial Y^2} \tag{33}$$

$$\frac{\partial\bar{T}_1^c(0,\beta)}{\partial Y}=\frac{1}{R}\left\{\bar{T}_1^c(0,\beta)-\bar{T}_1^d(0,\beta)\right\} \tag{34}$$

$$\frac{\partial\bar{T}_1^d(0,\beta)}{\partial Y}=\frac{\zeta}{R}\left\{\bar{T}_1^c(0,\beta)-\bar{T}_1^d(0,\beta)\right\} \tag{35}$$

$$\frac{\partial\bar{T}_1^d(-H,\beta)}{\partial Y}=\zeta\,\bar{Q}_1 \tag{36}$$

Thus, the problem is reduced to the determination of three pairs of functions $\bar{T}_0^c(Y,\beta)$, $\bar{T}_0^d(Y,\beta)$, $S_0(\beta)$ and $\bar{T}_1^c(Y,\beta)$, $\bar{T}_1^d(Y,\beta)$, $S_1(\beta)$ in Eqs. (25) and (26), which satisfy the boundary conditions (27)–(31) and (32)–(36), respectively.

5. Preview of the algorithm

Eqs. (25) and (26) with boundary conditions in (27)–(31) and (32)–(36) cannot be solved in closed form, and therefore we must resort to a numerical solution.

In the present work, an explicit finite difference Lagrangian scheme has been implemented. In this case, the zeroth-order solid phase $0<Y<S_0(t)$, is divided into a fixed number of elements N, so the space step size, $\delta=S_0/N$, increases with time due to the growth in $S_0(t)$. This permits the last node to be identified with the zeroth-order solid–liquid moving front at all times, but implies that the node locations move in time, necessitating the inclusion of convective terms in the updating algorithm for temperature. Thus, for example, the instantaneous zeroth-order solidified layer temperature field is represented by the temperatures at the $N+1$ points $Y=(i-1)\delta$, $i=1,2,\ldots,N+1$. The increase of the shell thickness S_0 during the next time increment τ is determined from the finite difference formulation of Eq. (28).

$$S_0^{j+1}=S_0^j+\frac{\tau}{2\delta}\left(3\bar{T}_{0_{N+1}}^j-4\bar{T}_{0_N}^j+\bar{T}_{0_{N-1}}^j\right) \tag{37}$$

after which the solidified layer temperatures at the interior nodes $i = 2, 3, \ldots, N$ are updated using the finite difference form of heat conduction equation (25)

$$\bar{T}_{0_i}^{j+1} = \bar{T}_{0_i}^{j} + \frac{\tau}{\varepsilon_1 \delta^2}\left(\bar{T}_{0_{i+1}}^{j} - 2\bar{T}_{0_i}^{j} + \bar{T}_{0_{i-1}}^{j}\right) \quad i = 2, 3, \ldots, N \tag{38}$$

which can be corrected using convective terms through

$$\bar{T}_{0_i}^{j+1} = \bar{T}_{0_i}^{j+1} + (i-1)\frac{\delta^{j+1} - \delta^{j}}{\delta^{j}}\left(\bar{T}_{0_{i+1}}^{j+1} - \bar{T}_{0_i}^{j+1}\right) \quad i = 2, 3, \ldots, N \tag{39}$$

The solidified layer temperatures at node $N+1$ remain at a constant value for all times in view of Eq. (27) and that at node 1 is updated through (29), which determines the first difference in the first element. Essentially, the same procedure is used to determine the evolution of the first-order solidified layer temperature field, using Eqs. (32)–(36).

The choice of an appropriate value for τ is motivated by the desire for computational efficiency, while retaining acceptable numerical convergence and stability. Extensive investigations were made into the effect of both space and time discretization to ensure that the final results are reliable. With the explicit scheme used here, the maximum time step for stability is proportional to $\varepsilon_1\delta^2$ and hence the stability requirement generally places a restriction on τ when good spatial accuracy is desired, necessitating very small values of δ. When the specific heats of the shell and mold materials are both considered in the model numerical stability of the scheme is satisfied if

$$\frac{\tau}{\varepsilon_1\delta^2} < 0.5, \qquad \frac{\tau}{\varepsilon_2\delta_d^2} < 0.5 \tag{40}$$

where δ_d and ε_2 are the space step size in the mold and the dimensionless specific heat of the mold material, respectively. At the beginning of the process, the solidified shell thickness and δ are very small, and therefore we need an extremely small time step that causes the numerical process to be very slow. However, S_0 and hence δ increases during the process, permitting the time step to be increased as the system evolves without loss of stability if the second condition given in Eq. (40) can be removed. Otherwise, the second condition in Eq. (40) places a very severe restriction on the time increment, τ, since δ_d remains constant during the process. Therefore, in the present study, extremely small initial value of δ is required to be used throughout the whole process.

With the algorithm described above, it is clearly not possible to start at the instant of first solidification, since at $S_0 = 0$, all the nodes would coincide. Instead, we need to use an asymptotic solution of the problem at small times to provide a suitable initial condition for the numerical algorithm at finite time. Fortunately, the limiting solution given in the next section, which assumes that diffusivities of the solidified shell and mold materials are both infinitely large, becomes progressively more accurate at small times, since the temperature drop across the solidified layer is small at the very beginning of the process. We can therefore start the process with a small but finite thickness, using the limiting solution given in the next section to define the initial values for the temperature fields in the solidified shell and the mold.

6. Limiting solution

It can be demonstrated that the solution for $\varepsilon_1 \to 0$ and $\varepsilon_2 \to 0$ is a limiting case of the present more general theory. This simplification permits the solution to be obtained in closed form and makes possible all the calculations to be performed analytically. The results of limiting case are useful in the development and checking of purely numerical solution of general case, as well as in providing a start-up solution for the general problem.

In physical terms, this simplifying assumption is equivalent to the statement that the casting and the mold materials have zero specific heat. In other words, the heat diffusivities of the casting and the mold materials are infinitely large. It then follows that Eqs. (25) approximate Laplace's equation and in view of the condition, $\partial s/\partial x \ll 1$, that the temperature profiles in the solidified layer and in the mold are linear in y. In this case, Eqs. (25) can easily be solved using the boundary conditions (27)–(31) with the result

$$\bar{T}_0^c(Y, \beta) = 1 + \bar{Q}_0[Y - S_0] \tag{41}$$

$$\bar{T}_0^d(Y, \beta) = 1 + \bar{Q}_0\left[\zeta Y - S_0 - R\right] \tag{42}$$

Substituting Eq. (41) into (28) and solving the ordinary differential equation for $S_0(\beta)$ we obtain the amplitude of the unperturbed solidification front as

$$S_0(\beta) = \bar{Q}_0\beta \tag{43}$$

The governing equation for the first order temperature field in the solid phase and in the mold can be solved remaining boundary conditions (32)–(36) with the result

$$\bar{T}_1^c(Y, \beta) = C_1(\beta)\sinh(Y) + C_2(\beta)\cosh(Y) \tag{44}$$

$$\bar{T}_1^d(Y, \beta) = C_3(\beta)\sinh(Y) + C_4(\beta)\cosh(Y) \tag{45}$$

where

$$C_1(\beta) = \frac{1}{\Delta}\left\{\zeta\,\bar{Q}_1\cosh(S_0) - S_1\bar{Q}_0\sinh(H)\right\} \tag{46}$$

$$C_2(\beta) = -\frac{S_1}{\Delta}\left\{\bar{Q}_0\zeta\cosh(H) + \bar{Q}_0 R\sinh(H) - \zeta\,\bar{Q}_1\sinh(S_0)\right\} \tag{47}$$

$$C_3(\beta) = \frac{\zeta}{\Delta}\left\{\zeta\,\bar{Q}_1\cosh(S_0) - S_1\bar{Q}_0\sinh(H)\right\} \tag{48}$$

$$C_4(\beta) = -\frac{\zeta}{\Delta}\left\{S_1\bar{Q}_0\cosh(H) + \bar{Q}_1\sinh(S_0) + \bar{Q}_1 R\cosh(S_0)\right\} \tag{49}$$

where

$$\Delta = \left\{\zeta\cosh(H) + R\sinh(H)\right\}\cosh(S_0) + \sinh(H)\sinh(S_0) \tag{50}$$

Finally, using Eqs. (33), (41), and (44) we can obtain a differential equation

$$S_1(\beta) = \frac{\cosh(S_0)}{\Delta}\left\{\zeta\,\bar{Q}_1\cosh(S_0) - S_1\bar{Q}_0\sinh(H)\right\} - \frac{S_1\sinh(S_0)}{\Delta}\left\{\bar{Q}_0\zeta\cosh(H) + \bar{Q}_0 R\sinh(H) - \zeta\,\bar{Q}_1\sinh(S_0)\right\} \quad (51)$$

for the amplitude of the perturbation in solidification front, with solution

$$S_1(\beta) = \frac{\zeta\,\bar{Q}_1 S_0(\beta)}{\bar{Q}_0\Delta} \quad (52)$$

Notice that when H goes to zero in the above equation, this limiting solution approaches

$$S_1(\beta) = \frac{\bar{Q}_1 S_0}{\bar{Q}_0\cosh(S_0)} \quad (53)$$

which is equal to the limiting solution for zero Stefan number given in Ref. [30] where the mold of zero thickness is assumed to be thermally rigid.

7. Results and discussions

The accuracy and convergence of the finite difference algorithm used in the present work are first validated with another finite difference algorithm developed for an unperturbed solution of the problem where $Q_1 = 0$, and excellent agreement between these two solutions has been obtained. The numerical algorithm has also been verified by comparing the computed results with the analytical limiting solution for the problem with zero specific heats of the casting and the mold materials. The analytical and the numerical solutions for small specific heats are seen to agree with each other within reasonable accuracy as shown in Fig. 2. Notice that the parameters ε_1 and ε_2 can be considered as describing the effect of finite thermal diffusivities, or equivalently, of the specific heats of the casting and the mold materials, respectively. The evolution of the mean layer thickness, $S_0(\beta)$ over an extended range of β for selected values of ε_1 is shown in Fig. 3. Note that increasing ε_1, i.e., increasing specific heat of the solidifying material, slows down the progress of the mean shell thickness. In other words, the solidified material with lower specific heat causes faster growth of the shell. Fig. 4 shows the effect of specific heat of the solidifying material on the growth of the perturbation in the solidification front for $\varepsilon_2 = 10$, $H = 10$, $R = 0.3$, and $\zeta = 2$. The results confirm the hypothesis of Yigit et al. [23] that materials with higher specific heat (or lower diffusivities) may be less prone to the growth instability. The results show that the maximum value of $S_1(\beta)$ occurs approximately $S_0(\beta) = 2$ for all values of ε_1 considered here. Recalling that $S_0(\beta) = ms_0(t)$ and that the wavelength of the perturbation in the x-direction is $2\pi/m$, we conclude that the maximum perturbation in the wave front oc-

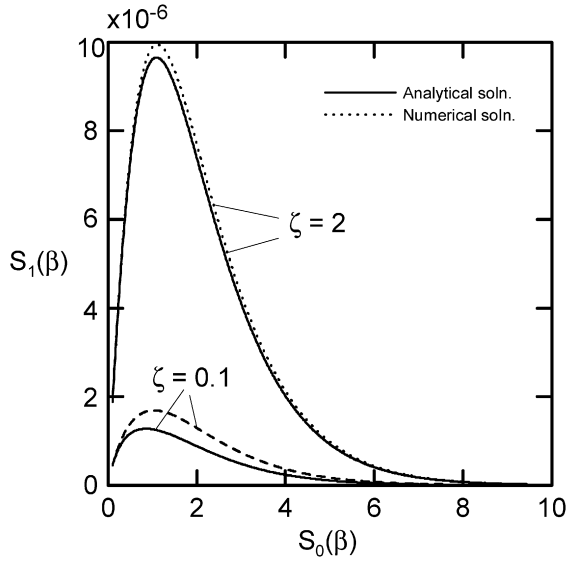

Fig. 2. Comparison of the numerical solutions to the analytical limiting solutions (solid lines) for perturbed solidification front as a function of $S_0(\beta)$ for $\zeta = 0.1$ (dashed line), and $\zeta = 2$ (dotted line). ($R = 0.3$, $H = 10$, $\varepsilon_1 = \varepsilon_2 = 0.01$.)

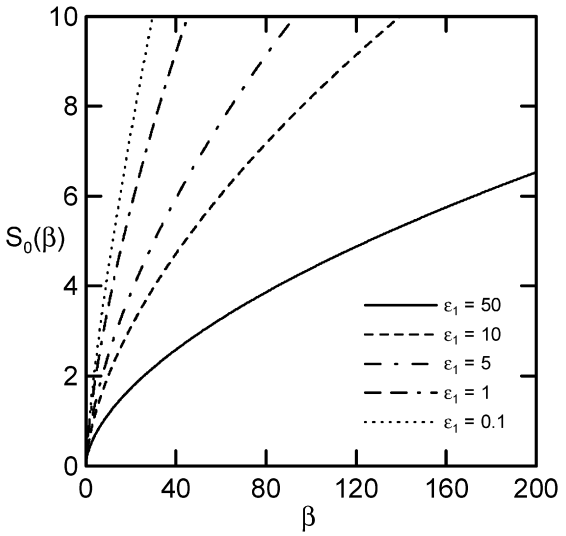

Fig. 3. Evolution of mean shell thickness as a function of dimensionless time, β for selected values of ε_1. ($R = 0.3$, $H = 10$, $\zeta = 2$, $\varepsilon_2 = 10$.)

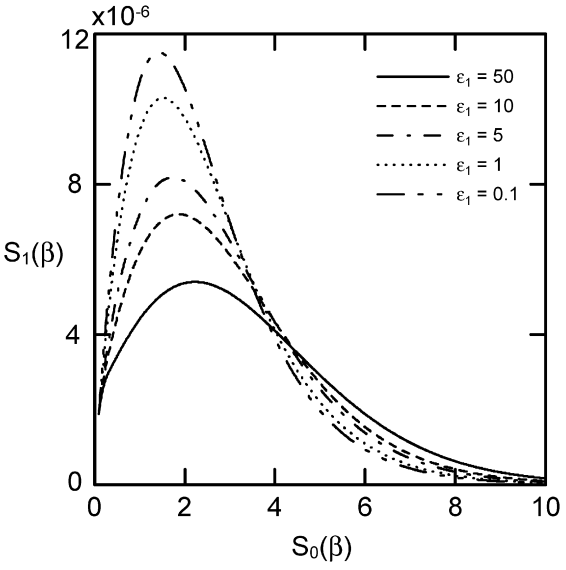

Fig. 4. Perturbation in solidification front as a function of $S_0(\beta)$ for selected values of ε_1. ($R = 0.3$, $H = 10$, $\zeta = 2$, $\varepsilon_2 = 10$.)

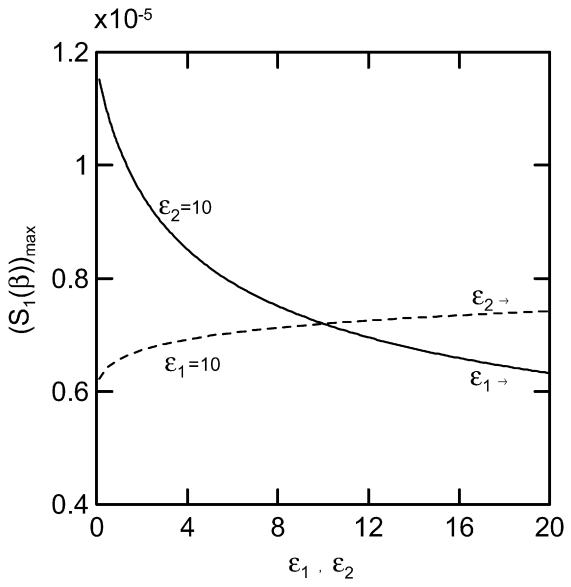

Fig. 5. Variation of maximum perturbation in solidification front with ε_1 and ε_2. ($R = 0.3$, $\zeta = 2$, $H = 10$.)

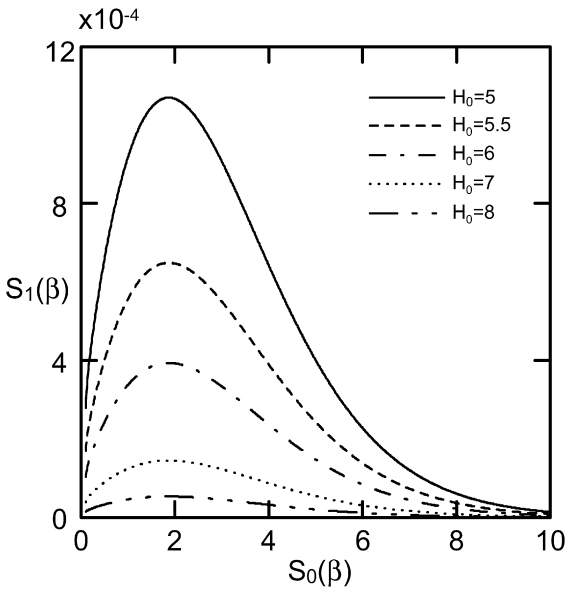

Fig. 6. Perturbation in solidification front as a function of $S_0(\beta)$ for selected values of H. ($R = 0.3$, $\zeta = 2$, $\varepsilon_1 = \varepsilon_2 = 10$.)

curs when the mean shell thickness $s_0(t)$ is approximately one third the wavelength of the perturbation. A physical explanation of this behavior is provided by the consideration that when $\beta > 3\pi$, the thickness of the solidified layer is greater than the wavelength of the perturbation, in which case variations in conditions at the shell/mold boundary will have little influence on those at the solidification front. The perturbation in solidification front therefore begins to decay when $\beta > 3\pi$ and later goes to its steady-state value approaching zero.

Fig. 5 shows the variation of the maximum values of perturbed solidification front, $S_1(\beta)_{\max}$, with specific heats of the shell and the mold materials, ε_1 and ε_2, for $0.1 \leqslant \varepsilon_1 \leqslant 20$ and $0.1 \leqslant \varepsilon_2 \leqslant 20$. The remaining process parameters were fixed at $R = 0.3$, $H = 10$, $\zeta = 2$, and ε_1 was fixed at 10 for the variation of $S_1(\beta)_{\max}$ with ε_2, and ε_2 was fixed at 10 for the variation of $S_1(\beta)_{\max}$ with ε_1. As it is seen, perturbation in solidification front reaches a higher maximum for larger values of ε_2. On the other hand, however, perturbation in solidification front reaches a higher maximum for smaller values of ε_1. Hence, we can conclude that the effect of ε_1 and ε_2 on the growth of perturbation in solidification front counteract each other.

Fig. 6 shows the variation of perturbed solidification front, $S_1(\beta)$, with $S_0(\beta)$ for selected mold thicknesses, H. The remaining process parameters were fixed at $R = 0.3$, $\varepsilon_1 = \varepsilon_2 = 10$, and $\zeta = 2$. The maximum of $S_1(\beta)$ increases rapidly as the mold thickness is reduced implying that probability of occurrence of unstable growth with a thinner mold is higher than a thicker one.

The data presented in previous figures was generated for a single set of process parameters and hence it is not possible to infer how the maximum of perturbed solidification front will change as the individual process parameters vary for a given set of process parameters. To explore the process parameters effect on $S_1(\beta)_{\max}$ Fig. 7 is reported. It examines the effect of R and ζ on $S_1(\beta)_{\max}$. It can be seen that these two parameters

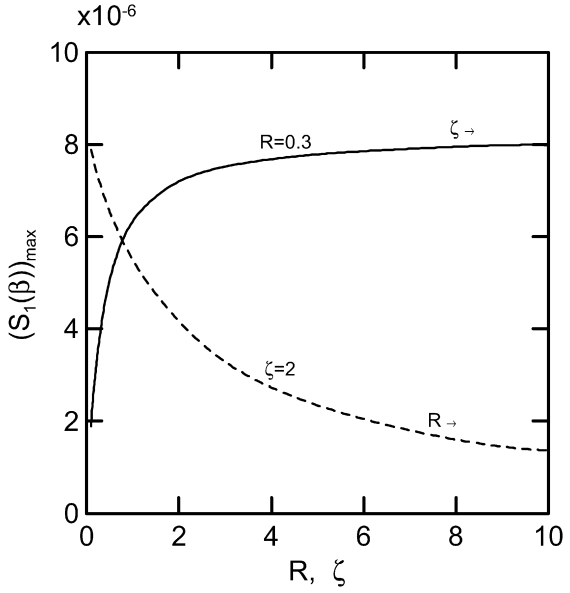

Fig. 7. Variation of maximum perturbation in solidification front as a function of dimensionless thermal contact resistance, R, and thermal conductivity ratio, ζ, for $H = 10$, $\varepsilon_1 = \varepsilon_2 = 10$.

have counteracting effects on the maximum of the perturbed solidification front. When R is varying ζ is fixed at 2. When ζ is varying R is fixed at 0.3. The remaining process parameters were fixed at $H = 10$ and $\varepsilon_1 = \varepsilon_2 = 10$. Fig. 8 shows the position of the solid-melt interface at various values of the dimensionless time, β, at $R = 0.1$, $H = 0.1$, $\zeta = 10$, ε_1, and $\varepsilon_2 = 100$. As the solidification proceeds the shell thickness nonuniformity increases. If solidification is interrupted, periodic thickness nonuniformities at the freezing front will be observed. If solidification is allowed to proceed, however, the nonuniformities tend to die out as the freezing front morphology becomes less dependent upon the mold–shell interface due

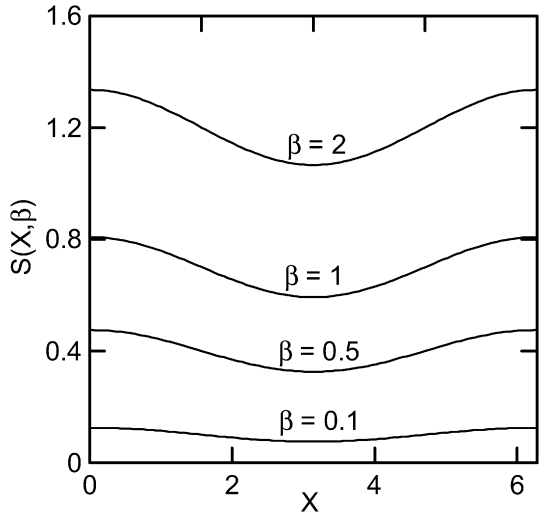

Fig. 8. Growth of the solidified shell with a sinusoidal variation in the heat flux at selected dimensionless time, β. ($R = 0.3$, $H = 0.1$, $\zeta = 10$, $\varepsilon_1 = 1$, $\varepsilon_2 = 100$.)

to the ever-thickening shell. It should be noted that this theoretical result is supported by many experimental observations of thermomechanical growth instability in casting processes [29].

Current work on this problem is focused on a fully coupled version of the present problem that includes the effect of mechanical problems (i.e., stress fields in the solidified shell thickness and the mold, and contact pressure variations in the mold–shell interface). This requires that the thermoelastic stress fields in the solidified shell thickness and the mold to be added into the thermal fields presented in this work. The present theory does not account for this important phenomenon and, hence, predictions made about the growth instability here are clearly restrictive. It is anticipated that the fully coupled version of the present problem may provide conclusive demonstration of the growth instability mechanism observed in many casting experiments.

8. Conclusions

The heat conduction part of the solidification problem has been investigated in which one dimensional solidification process occurs on a plane mold of finite thickness. In particular, numerical solutions have been obtained for the advance of the solid/melt boundary. The effect of specific heats of the solidified shell and the mold materials was also investigated. It was demonstrated that the solidified shell material with higher specific heat might result in slower growth of perturbation in solidification front, whereas the mold material with higher specific heat may cause faster growth of the shell thickness perturbation. The effects of remaining process parameters such as mold thickness, thermal contact resistance at the mold–shell interface, and thermal conductivity ratio between the solidified shell and the mold have also been studied in detail.

We have also briefly discussed the limiting solution for $\varepsilon_1 = \varepsilon_2 = 0$, in which the zeroth order temperature profiles in the solid and in the mold are linear in y. This simplification permits the problem to be solved analytically.

The present model developed in this paper is currently being extended to incorporate the thermal stress fields which are coupled with the temperature fields along the mold–shell interface through a pressure-dependent thermal contact resistance. In this case, changes in the local mold–shell interface pressure will be reflected in the local casting thickness, which is not captured in the physics of the present model. In particular, the coupling of interface pressure and interface heat flux is being developed in order to study the impact of selected process parameters such as thermal capacities of the shell and mold materials, mold thickness, conductivity ratios between the shell and mold materials, and the wavelength of the applied heat flux on the morphology of the solid–liquid interface. The present model is also being extended to study the impact of engineered mold surface textures since it is believed that the mold surface topography has a great influence on the cast surface quality, microstructure, and thickness uniformity. It is also believed that air gap formations and their locations at the solid–mold interface have a significant effect on the growth instability. The present work is also being developed to investigate gap nucleation process and to determine optimum mold surface wavelength or range of wavelengths which correspond to the highest growth rate and dominate the behavior of the growth instability. The results will be reported in forthcoming articles.

References

[1] H.S. Carslaw, J.C. Jaeger, Conduction of Heat in Solids, second ed., Oxford Univ. Press, London, UK, 1956, pp. 282–296.
[2] M.N. Ozisik, Boundary Value Problems Heat Conduction, Dover Publications, Inc., New York, 1968, pp. 301–338.
[3] M.N. Ozisik, Heat Conduction, Wiley, New York, 1980, pp. 397–438.
[4] T.R. Goodman, The heat balance integral and its application to problems involving a change of phase, Trans. ASME 80 (1958) 335–342.
[5] N. Sadoun, E.K. Khider Si-Ahmed, P. Colinet, On the refined integral method for the one-phase Stefan problem with time dependent boundary conditions, Appl. Math. Model. 30 (2006) 531–544.
[6] H.-S. Ren, Application of the heat-balance integral to an inverse Stefan problem, Int. J. Thermal Sci. 46 (2007) 118–127.
[7] J. Mennig, M.N. Ozisik, Coupled integral equation approach for solving melting or solidification, Int. J. Heat Mass Transfer 28 (1985) 1481–1485.
[8] R.M. Cotta, M.N. Ozisik, J. Mennig, Coupled integral equation approach for solving phase-change problems in a finite slab, J. Franklin Inst. 327 (1990) 225–234.
[9] A. Lazaridis, A numerical solution of the multi-dimensional solidification (or melting) problem, Int. J. Heat Mass Transfer 13 (1970) 1459–1477.
[10] S. Savovic, J. Caldwell, Finite difference solution of one-dimensional Stefan problem with periodic boundary conditions, Int. J. Heat Mass Transfer 46 (2003) 2911–2916.
[11] W. Rolph III, K.-J. Bathe, An efficient algorithm for analysis of nonlinear heat transfer with phase changes, Int. J. Numer. Methods Engrg. 18 (1982) 119–134.
[12] R.T. Tenchev, J.A. Mackenzie, T.J. Scanlon, M.T. Stickland, Finite element moving mesh analysis of phase change problems with natural convection, Int. J. Heat Fluid Flow 26 (2005) 597–612.
[13] R.I. Pedroso, G.A. Domoto, Exact solution by perturbation method for planar solidification of a saturated liquid with convection at the wall, Int. Heat Mass Transfer 16 (1973) 1816–1819.
[14] R.I. Pedroso, G.A. Domoto, Perturbation solutions for spherical solidification of saturated liquids, J. Heat Transfer 19 (1973) 42–46.
[15] K. Stephan, B. Holzknecht, Perturbation solutions for solidification problems, Int. Heat Mass Transfer 19 (1976) 597–602.

[16] J. Caldwell, Y.Y. Kwan, On the perturbation method for Stefan problem with time-dependent boundary conditions, Int. J. Heat Mass Transfer 46 (2003) 1497–1501.
[17] Z. Yang, M. Sen, S. Paolucci, Solidification of a finite slab with convective cooling and shrinkage, Appl. Math. Model. 27 (2003) 733–762.
[18] Ch. Charach, M. Huleihil, Y. Zarmi, Perturbative analysis of planar phase change processes with time dependent temperature at the boundary, J. Appl. Phys. 64 (1988) 4832–4837.
[19] M.M. Yan, P.N.S. Huang, Perturbation solutions to phase change problem subjected to convection and radiation, ASME J. Heat Transfer 101 (1979) 96–100.
[20] S. Weinbaum, L.M. Jiji, Singular perturbation theory for melting or freezing in finite domains initially not at fusion temperature, ASME J. Appl. Mech. 44 (1977) 25–30.
[21] S. Kharche, J.A. Howarth, The inward solidification of a liquid cylinder with periodic axial perturbation of the boundary temperature or heat flux, Int. Comm. Heat Mass Transfer 27 (2000) 903–912.
[22] S. Kharche, J.A. Howarth, The inward solidification of a liquid cylinder with periodic axial perturbation of the boundary geometry, and constant boundary temperature or heat flux, Int. Comm. Heat Mass Transfer 27 (2000) 913–923.
[23] F. Yigit, Perturbation solution for solidification of pure metals on a sinusoidal mold surface, Int. J. Heat Mass Transfer, in press.
[24] J. Caldwell, Y.Y. Kwan, Numerical methods for one-dimensional Stefan problems, Commun. Numer. Meth. Engrg. 20 (2004) 535–545.
[25] E. Javierre, C. Vuik, F.J. Vermolen, S. van der Zwaag, A comparison of numerical models for one-dimensional Stefan problems, J. Comput. Appl. Math. 192 (2006) 445–459.
[26] S. Jana, S. Ray, F. Durst, A numerical method to compute solidification and melting processes, Appl. Math. Model. 31 (2007) 93–119.
[27] O. Richmond, N.C. Huang, Interface instability during unidirectional solidification of a pure metal, in: Proc. 6th Canadian Congress of Applied Mechanics, Vancouver, 1977, pp. 453–454.
[28] F. Yigit, J.R. Barber, Effect of Stefan number on thermoelastic instabilities in unidirectional solidification, Int. J. Mech. Sci. 36 (8) (1994) 707–723.
[29] H. Murakami, M. Suzuki, T. Kitagawa, S. Miyahara, Control of uneven solidified shell formation of hypo-peritectic carbon steels in continuous casting mold, J. Iron Steel Inst. Japan 78 (1992) 105–112.
[30] F. Yigit, N.-Y. Li, J.R. Barber, Effect of thermal capacity on thermoelastic instability during the solidification of pure metals, J. Thermal Stresses 16 (1993) 285–309.
[31] O. Richmond, L.G. Hector Jr., J.M. Fridy, Growth instability during nonuniform directional solidification of pure metals, ASME J. Appl. Mech. 57 (1990) 529–536.
[32] N.-Y. Li, J.R. Barber, Thermoelastic instability in planar solidification, Int. J. Mech. Sci. 33 (1991) 945–959.
[33] F. Yigit, L.G. Hector Jr., Critical wavelengths for gap nucleation in solidification. Part 1: Theoretical methodology, ASME J. Appl. Mech. 67 (2000) 66–76.
[34] F. Yigit, L.G. Hector Jr., Critical wavelengths for gap nucleation in solidification. Part 2. Results for selected mold–shell material combinations, ASME J. Appl. Mech. 67 (2000) 77–86.
[35] L.G. Hector Jr., J.A. Howarth, O. Richmond, W.-S. Kim, Mold surface wavelength effect on gap nucleation in solidification, ASME J. Appl. Mech. 67 (2000) 155–164.
[36] F. Yigit, Existence of critical wavelength for gap nucleation in solidification on a rigid mold, ASME J. Appl. Mech. 71 (2004) 96–108.
[37] F. Yigit, L.G. Hector Jr., O. Richmond, A theoretical investigation of pure metal solidification on a deformable mold in the absence of interfacial coupling, J. Thermal Stresses 25 (2002) 773–809.